Research Square

Preprints are preliminary reports that have not undergone peer review.
They should not be considered conclusive, used to inform clinical practice,
or referenced by the media as validated information.

Low-intensity vibration improves the yield and functional quality of tumor-infiltrating lymphocytes for personalized cellular immunotherapy

Geofrey F. Soko

filbert.soko@orci.or.tz

Ocean Road Cancer Institute

Benson K. Kosgei

Jiangxi University of Chinese Medicine

Stephene S. Meena

Jiangxi University of Chinese Medicine

Wen Zheng

Jiangxi University of Chinese Medicine

Yuting Zhong

Jiangxi University of Chinese Medicine

Xinju Hou

Nanchang Hongdu Hospital

Ying Jing Ng

Jiangxi University of Chinese Medicine

Ying Wang

Affiliated Hospital of Jiangxi University of Chinese Medicine

Qisheng Cao

Affiliated Hospital of Jiangxi University of Chinese Medicine

Liu Yuan

Affiliated Hospital of Jiangxi University of Chinese Medicine

Li Wang

Jiangxi University of Chinese Medicine

Puying Luo

Jiangxi Maternal and Child Health Hospital

Ray P.S. Han

Jiangxi University of Chinese Medicine

Article

Keywords:

Posted Date: November 25th, 2026

DOI: https://doi.org/10.21203/rs.3.rs-11710852/v1

License: This work is licensed under a Creative Commons Attribution 4.0 International License.
Read Full License

Additional Declarations: No competing interests reported.

Low-intensity vibration improves the yield and functional quality of tumor-infiltrating lymphocytes for personalized cellular immunotherapy

Geofrey F. Soko[1,2,7]✉, Benson K. Kosgei[1,7], Stephene S. Meena[1,2,7], Wen Zheng[1], Yuting Zhong[1], Xinju Hou[3], Ying Jing Ng[1], Ying Wang[4], Qisheng Cao[5], Yuan Liu[5], Li Wang[1]✉, Puying Luo[6]✉, Ray P.S. Han[1]✉

The efficacy of TIL tumor-infiltrating lymphocyte (TIL) therapy is highly dependent on the quantity and therapeutic quality of infused cells. Although bio*chemical* stimulation is widely used to enhance TIL expansion and modulate phenotype, it has several limitations, including limited specificity, poor scalability, and high cost. In contrast, bio*mechanical* stimulation is relatively inexpensive and offers precise tunability. Here, we explored low-intensity vibration (LIV) as a biomechanical tool to enhance TIL expansion and functionality. Quantitatively, LIV increased TIL yield by an average of 1.3-fold relative to non-LIV controls. Qualitatively, LIV enriched expanded TILs with $CD8^+$ T cells while simultaneously decreasing PD-1^+ exhausted $CD4^+$ and $CD8^+$ cell subsets. Functionally, LIV-treated TILs induced greater tumor cell apoptosis and secreted higher levels of effector cytokines (IFN-γ, TNF-α, and IL-2). Mechanistically, LIV upregulated pro-inflammatory common γ-chain (γc) cytokines (IL-4, IL-7, and IL-15), which promote $CD8^+$ T cell proliferation, survival, and effector function. These findings underscore LIV as a relatively simple, scalable, and cost-effective biomechanical intervention to enhance T cell fitness, positioning it as a promising adjunct to existing TIL biomanufacturing protocols for adoptive cell therapy.

Cellular immunotherapies, which involve the adoptive transfer of ex vivo expanded and/or modified autologous or allogeneic immune cells, hold considerable promise for treating solid tumors. TIL therapy, in particular, offers unique advantages – including its ability to target a diverse repertoire of tumor antigens, superior homing and infiltration capabilities, and an excellent safety profile[1]. TIL therapy has demonstrated notable success in advanced melanoma

[1]Jiangxi Engineering Research Center for Translational Cancer Technology, Jiangxi University of Chinese Medicine, Nanchang, Jiangxi, China 330004. [2]Dept of Clinical Oncology, Ocean Road Cancer Institute, P.O. Box 3592, Dar es Salaam, Tanzania. [3]Dept of Rehabilitation, Nanchang Hongdu Hospital of Chinese Medicine, 1399 Diezihu Road, Honggutan, Nanchang, Jiangxi, China 330008. [4]Dept of Pathology, The Affiliated Hospital of Jiangxi University of Chinese Medicine, Nanchang, Jiangxi, China 330006. [5]Dept of Bone and Soft Tissue Tumors, The Affiliated Hospital of Jiangxi University of Chinese Medicine, Nanchang, Jiangxi, China 330006. [6]Dept of Gynecologic Oncology, Jiangxi Maternal and Child Health Hospital, Nanchang, Jiangxi, China 330038. [7]These authors contributed equally: Geofrey F. Soko, Benson K. Kosgei, Stephene S. Meena.
✉e-mail: filbert.soko@orci.or.tz; 250511832@qq.com, ray-han@jxutcm.edu.cn

refractory to immune checkpoint and BRAF/MEK inhibitors[2] and is emerging as a viable option for other solid malignancies, such as non-small cell lung cancer (NSCLC), ovarian cancer, and head and neck cancers[3]. The efficacy of TIL therapy depends on several factors, including the total number of infused cells, the proportion and clonal diversity of $CD8^+$ T cells within the TIL product, the tumor reactivity of infused lymphocytes, and their proliferative capacity and persistence in vivo[4,5]. However, generating TIL products that embody all these desirable characteristics remains a challenge. Key limitations include: insufficient TIL expansion from *cold* tumors due to poor T cell infiltration and functional impairment; T cell exhaustion during prolonged ex vivo expansion; and variability in product quality of bespoke biomanufacturing protocols[1,6]. These hurdles contribute to the difficulty in translating the success of melanoma TIL therapy to broader solid malignancies[7].

Biochemical strategies employing soluble or surface-engineered factors, such as cytokines, co-stimulatory molecules, immune checkpoint inhibitors, and metabolic modulators, are ubiquitously used to enhance TIL expansion from solid tumor specimens. While IL-2 is indispensable as a T cell growth factor, supplementation with IL-7, IL-15, or IL-21 has been shown to promote the expansion of less-differentiated, memory-like TILs with enhanced cytotoxicity and in vivo persistence[8-10]. These cytokine effects on TIL expansion are often amplified via costimulatory signals such as CD28[11], 4-1BB[12], or OX40[13] ligands, which synergistically enhance proliferation and cytotoxicity. Further, metabolic reprogramming has emerged as a key strategy to enhance TIL function. Approaches such as boosting mitochondrial activity or reducing oxidative stress with antioxidants such as N-acetylcysteine have been shown to improve TIL viability and prevent exhaustion and senescence[14,15]. Concurrent immune checkpoint blockade with agents like anti-PD-1 or anti-CTLA-4 further helps sustain the functional capacity and tumor reactivity of expanded TILs[16,17]. These biochemical strategies, although widely utilized in TIL biomanufacturing to improve yields and enhance tumor reactivity, face several limitations, including a lack of specificity, risks of contaminating TIL products with residual reagents, significant challenges in scaling up the complex cocktail-based processes, and prohibitively high costs[18].

T cell activation, proliferation, and effector function are governed not only by biochemical cues but also by biomechanical forces generated at the immunological synapse (IS) during their interactions with antigen-presenting cells (APCs)[19-21]. The intrinsic mechanical forces at the IS induce conformational changes in the T cell receptor (TCR) and lymphocyte function-associated antigen-1 (LFA-1), triggering downstream signaling pathways essential for T cell responses[22]. Beyond these intrinsic forces, externally applied low-magnitude mechanical

forces can further trigger T cells by amplifying forces at the IS[23] and activating mechanosensors such as Piezo1[24]. Highly expressed on the plasma membrane and intracellular vesicles of resting T cells, Piezo1 mediates calcium influx and calpain activation[25], leading to the induction of nuclear factor of activated T cells (NFAT), zeta-chain-associated protein kinase-70 (ZAP-70), and nuclear factor kappa-light-chain-enhancer of activated B cells (NF-κB), key regulators of T cell activation[24,26]. Moreover, Piezo1 signaling restrains regulatory T cell (Treg) expansion and downregulates PD-1 on $CD8^+$ T cells, while preserving effector $CD8^+$ T cell function[27,28]. In the context of TIL biomanufacturing, these observations suggest potential benefits of external mechanical signals to increase TIL yields and enrich the TIL product with functionally competent T cells.

In this work, we harnessed low-intensity vibrations (LIV) as an external mechanical cue to augment the expansion of TILs from tumor specimens and to modulate the phenotypes of expanded TILs, thereby enhancing their therapeutic quality for adoptive cell therapy. We demonstrate that LIV significantly improves TIL expansion and favorably reshapes the cellular composition of the TIL product, increasing the proportion of $CD8^+$ T cells, reducing PD-1 expression, and enhancing both cytotoxicity and effector cytokine secretion. These findings provide a rationale for integrating LIV into TIL expansion protocols to improve both TIL yields and the therapeutic quality of the final product.

Results

Optimization of LIV parameters for TIL expansion from tumor biospecimens

To optimize LIV parameters for TIL expansion, tumor fragments were cultured in TIL expansion medium for 2 days to allow TIL extravasation, followed by 5 days of LIV treatment at 20, 30, 40, or 50Hz (Fig. 1A). TIL yields increased in a frequency-dependent manner, rising from 0Hz to a peak at 40 Hz, then declining at 50 Hz (Fig. 1B). Fold expansion, calculated as the ratio of the final TIL count to the initial viable TIL plated, followed the same trend, with maximum expansion at 40 Hz (Fig. 1C). No significant differences in TIL viability (Fig. 1D) or average cell diameter (Fig. 1E) were observed between the static control and any of the tested LIV frequencies. Based on these results, we selected 40 Hz as the optimal frequency for all subsequent experiments.

Applying this optimized parameter to pre-Rapid Expansion Protocol (pre-REP) expansion of TILs from 10 soft tissue sarcoma specimens yielded a significant and consistent increase in TIL output (Fig. 1F), with LIV-treated TILs (L-TILs) achieving an average fold expansion of 1.3 ± 0.37 compared to controls (C-TILs) (Fig. 1G).

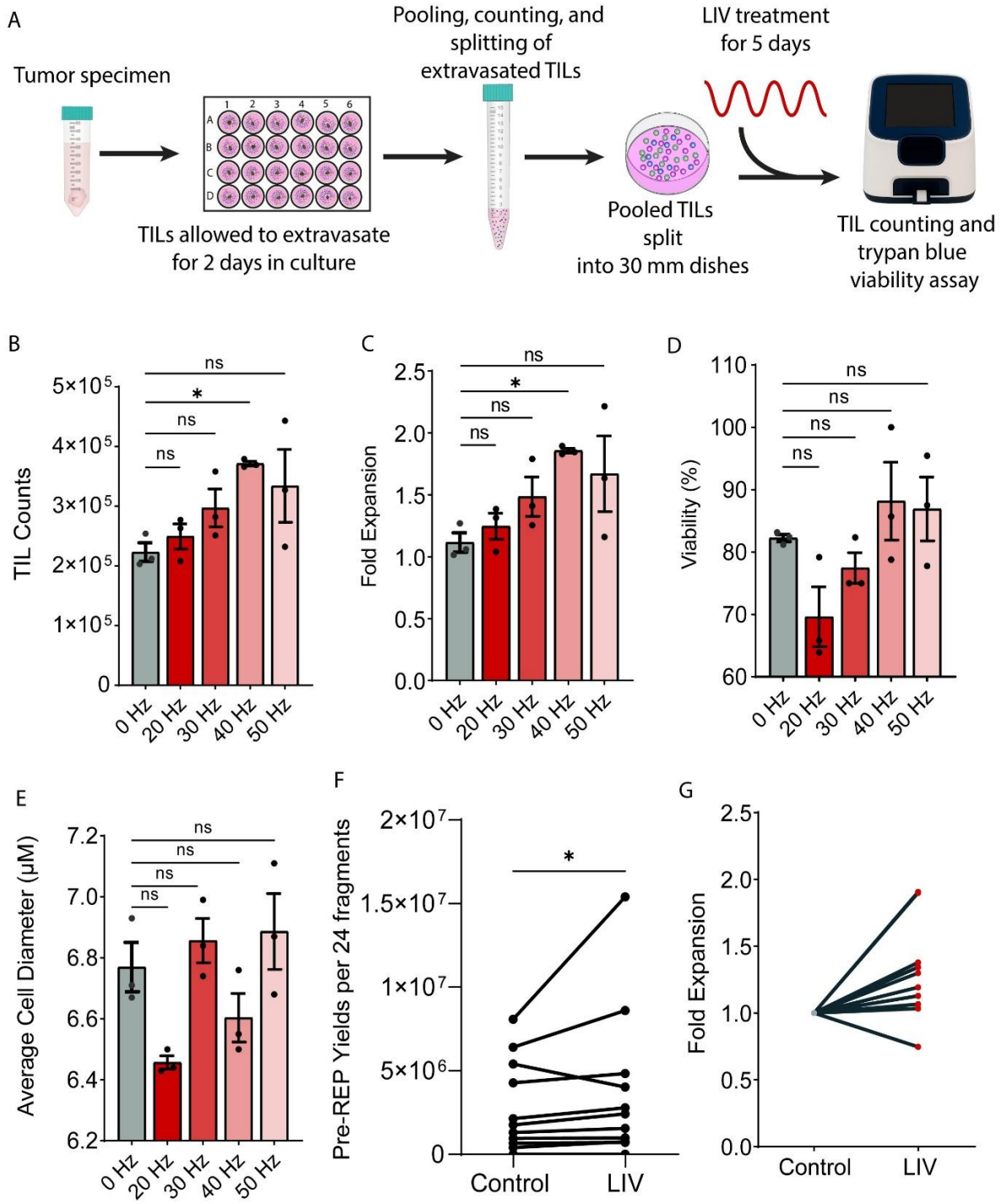


Fig. 1 | LIV enhances the ex vivo expansion of TILs. A Experimental workflow. Tumor fragments (~ 1 mm³) were cultured for two days to allow TIL extravasation. The extravasated TILs were pooled, counted, and seeded at 1×10^5 viable cells per 35 mm dish, followed by five days of LIV exposure at varying frequencies. After seven days in culture, expanded TILs were harvested for enumeration and viability assessment. **B** LIV at 40 Hz maximizes TIL yield ($*p < 0.05$). Total viable TIL counts were determined following exposure to the indicated LIV frequencies. **C** LIV at 40 Hz enhances TIL expansion capacity ($*p < 0.05$). Fold expansion was calculated by normalizing Day 7 TIL count to the initial 1×10^5 input cells. **D** LIV does not adversely affect TIL viability. A modest increase in viability was observed at 40 Hz, though this did not reach statistical significance (ns, not significant). Cell viability was assessed by trypan blue exclusion across all conditions. **E** Average cell diameter of TILs exposed to different LIV frequencies and the changes were insignificant. **F** LIV at 40 Hz consistently expands TILs from intact tumor fragments of ten independent patients. The specimens were cultured for ten days with or without LIV (40 Hz, applied in two daily 20-m bouts, separated by a 2-h interval). The graph displays the total TIL yield per 24 tumor fragments of each patient, with connected points representing matched samples ($*p < 0.05$). **G** LIV enhances TIL expansion from intact fragments. Fold expansion of LIV-treated TILs (L-TILs) was calculated relative to matched static controls (C-TILs). All data are presented as Mean ± SEM from triplicate experiments.

LIV enriches TIL products with CD8$^+$ T cells without affecting Treg proportions

Phenotypic analysis of expanded TIL populations by flow cytometry revealed that while the proportions of CD4$^+$ T cells were comparable between C-TILs and L-TILs (Fig. 2A), L-TILs contained significantly higher proportions of CD8$^+$ T cells than paired controls expanded from the same tumor specimen (Fig. 2B). This shift toward a more cytotoxic phenotype suggests that LIV may improve the antitumor potency of the final TIL product. Importantly, this enrichment occurred without significantly altering the CD8$^+$/CD4$^+$ ratio (Fig. 2C) or the proportion of immunosuppressive FOXP3$^+$CD4$^+$ Tregs (Fig. 2D), indicating that LIV does not promote the expansion of this potentially detrimental population. These findings highlight the potential of LIV to improve the therapeutic quality of TIL products.

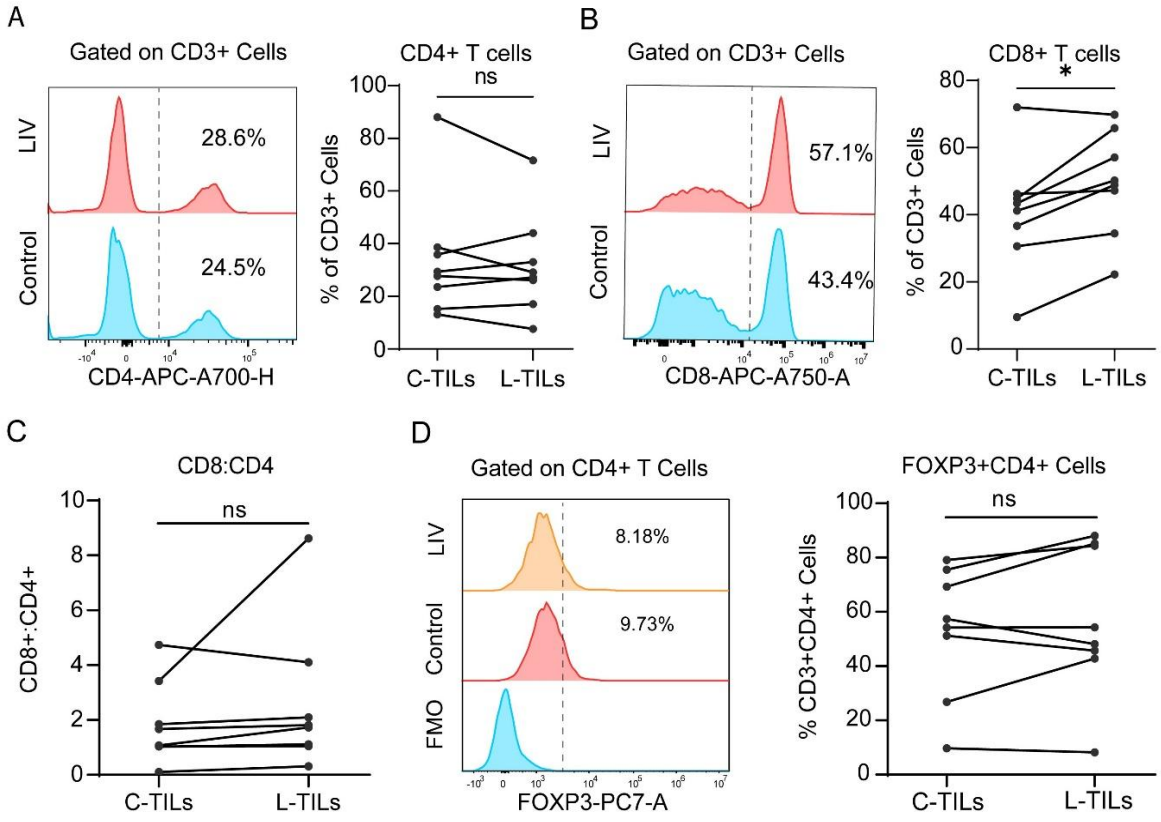


Fig. 2 | LIV exposure selectively enriches CD8$^+$ T cells in expanded TIL products. TILs expanded from eight independent patient tumor specimens under static control (C-TIL) or 40 Hz LIV (L-TIL) conditions were harvested and analyzed by flow cytometry to assess T-cell subset composition. **A** LIV exposure did not alter the proportion of CD4$^+$ T cells. Following LIV treatment, representative histogram overlays (left) and paired analysis of eight patient samples (right) showed that changes in CD4$^+$ population were insignificant (ns). **B** LIV significantly increases the proportion of CD8$^+$ T cells. Following LIV treatment, representative histogram overlays (left) showed a shift toward a higher CD8$^+$ population in L-TILs. Paired comparisons across eight patients (right) showed a statistically significant increase in CD8$^+$ T cells (*$p < 0.05$). **C** The CD8/CD4 ratio shows an increasing trend. While the calculated ratio of CD8$^+$-to-CD4$^+$ T cells were elevated in L-TILs, the difference did not attain statistical significance (ns). **D** LIV does not affect the proportion of Tregs. The proportion of immunosuppressive FOXP3$^+$CD4$^+$ Tregs cells within the expanded product (right) was comparable and paired analysis (left) confirmed the change was statistically insignificant (ns).

LIV reduces PD-1 expression in both $CD4^+$ and $CD8^+$ T cells in expanded TIL products

To determine whether LIV influences the exhaustion status of expanded TILs, we quantified the proportions of T cells expressing PD-1 and CTLA-4 in both C-TILs and L-TILs. Notably, L-TILs exhibited significantly lower proportions of both $PD\text{-}1^+CD4^+$ (Fig. 3A) and $PD\text{-}1^+CD8^+$ (Fig. 3B) T cells compared to their matched controls ($*p < 0.05$), suggesting that LIV may yield a less exhausted, potentially more functional TIL product. In contrast, CTLA-4 expression was comparatively low across all samples, and the proportions of $CTLA\text{-}4^+CD4^+$ (Fig. 3C) and $CTLA\text{-}4^+CD8^+$ (Fig. 3D) T cells did not differ significantly between C-TILs and L-TILs. These findings indicate that LIV selectively reduces the exhausted $PD\text{-}1^+$ population without broadly altering CTLA-4 expression.

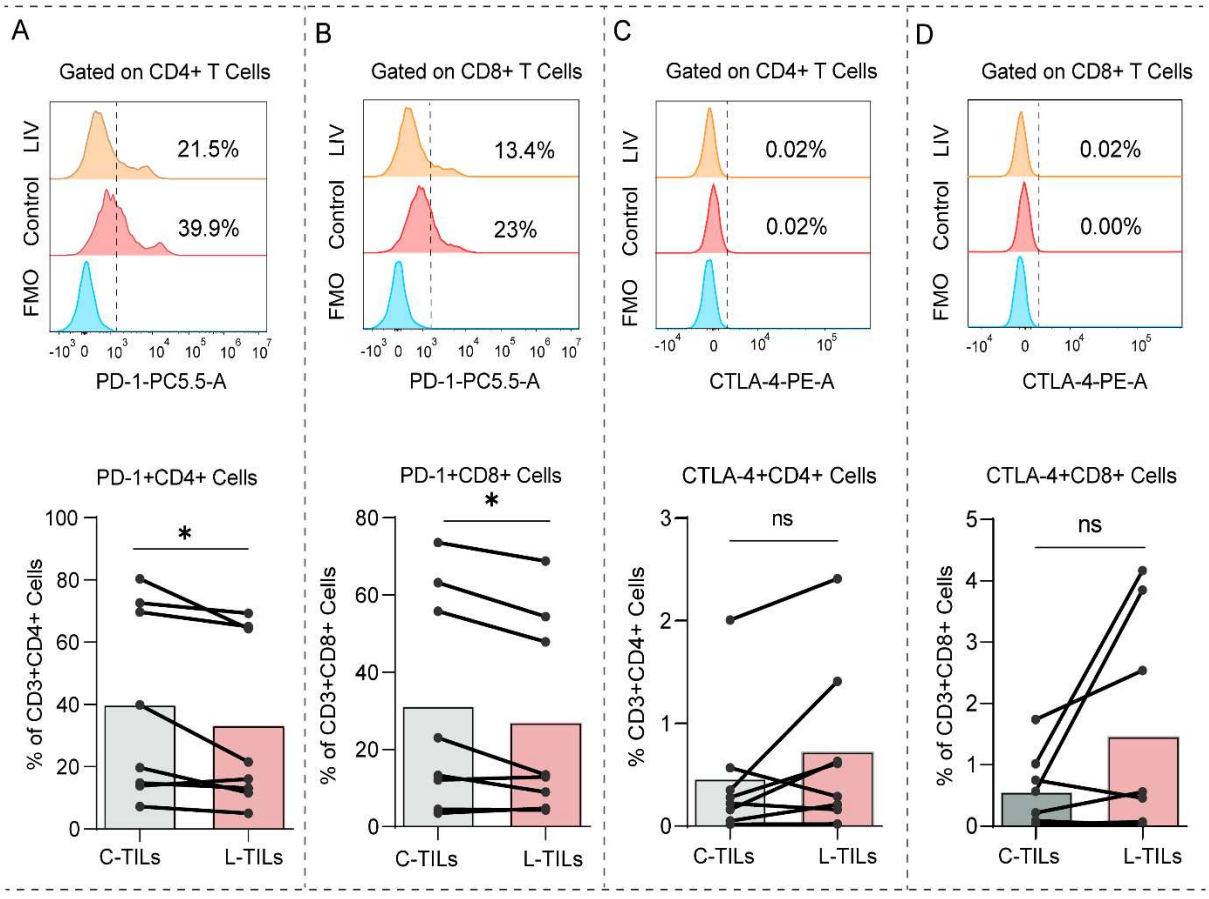


Fig. 3 | LIV reduces the proportion of exhausted $PD\text{-}1^+$ T cells in expanded TILs. To assess exhaustion markers PD-1 and CTLA-4, expanded TILs from eight independent patient tumor specimens were harvested and analyzed by flow cytometry. These TILs were derived from either static control (C-TIL) or 40 Hz LIV (L-TIL) conditions. **A**, **B** Histogram overlays (top) show a reduction in $PD\text{-}1^+$ in L-TILs (bottom), following LIV exposure. Paired analysis confirmed a statistically significant reduction in PD-1 positivity in (**A**) $CD4^+$ and (**B**) $CD8^+$ T cell proportions ($*p < 0.05$). **C**, **D** Histogram overlays (top) show no change in $CTLA\text{-}4^+$ in L-TILs (bottom), following LIV exposure. Paired analysis confirmed a statistically insignificant change in CTLA-4 positivity in (**C**) $CD4^+$ and (**D**) $CD8^+$ T cell proportions (ns).

LIV synergizes with PD-1 blockade to enhance TIL expansion and promote an enriched $CD8^+$ phenotype

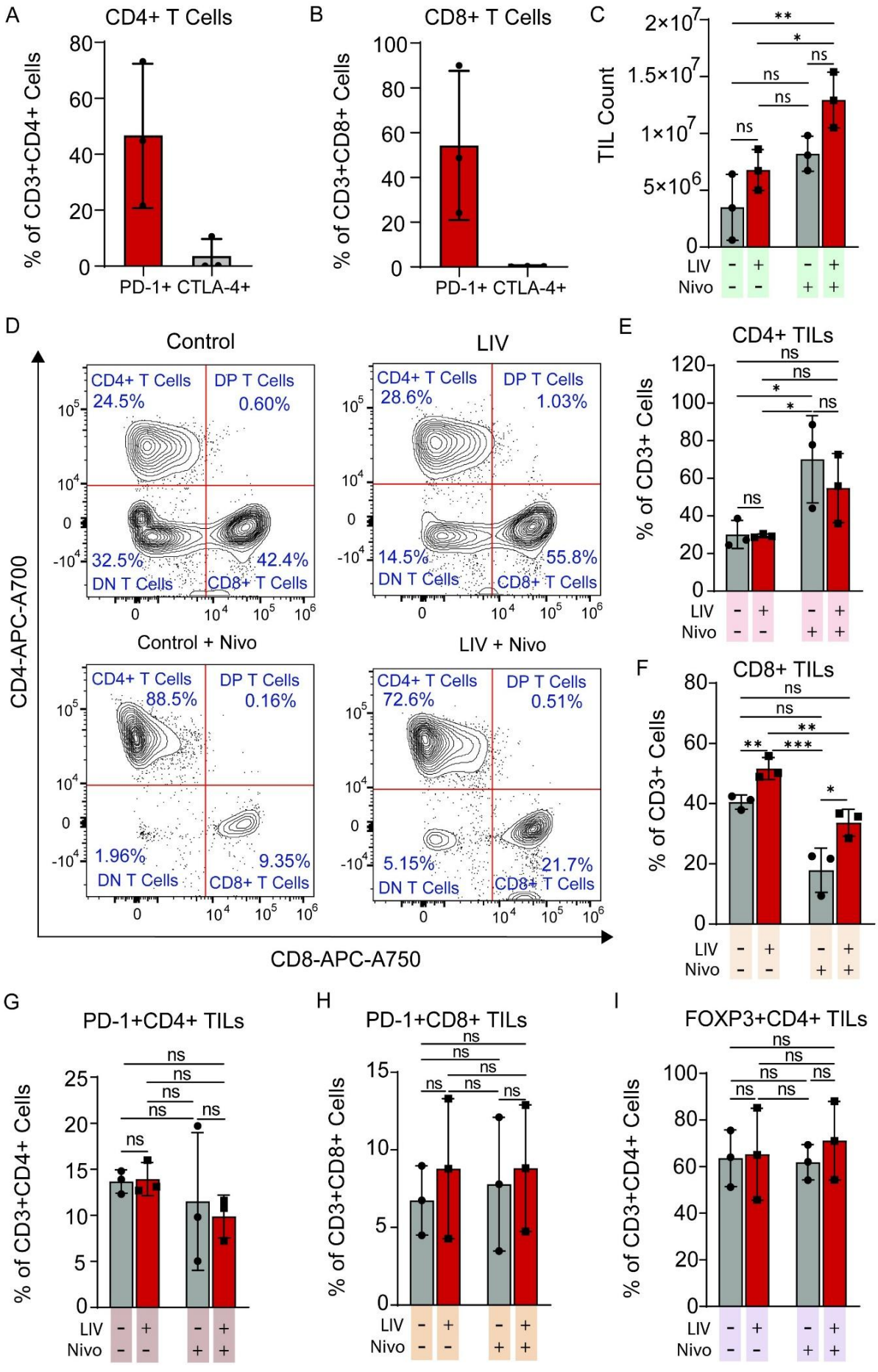
Previously, we showed that L-TILs contained significantly lower proportions of $PD\text{-}1^+CD4^+$ and $PD\text{-}1^+CD8^+$ T cells, suggesting that LIV reduces T cell exhaustion. Given the high PD-1 expression observed in both $CD4^+$ and $CD8^+$ T cells from tumor digests (Fig. 4, A and B), we next investigated whether PD-1 blockade could enhance TIL expansion and synergize with LIV. PD-1 blockade was implemented by supplementing the expansion medium with 10 μg/mL nivolumab (nivo).

TIL yields were significantly higher in L-TILs when LIV was combined with PD-1 blockade (nivo) compared to C-TILs with either PD-1 blockade alone or no PD-1 blockade (Fig. 4C), suggesting a synergistic link between LIV and PD-1 blockade. Nivo supplementation without LIV significantly increased the proportion of $CD4^+$ T cells in expanded TILs (Fig. 4, D and E), while the addition of LIV to PD-1 blockade lowered the CD4+ T cell proportions to levels that were not significantly different from the no PD-1 blockade condition (Fig. 4E).

More pronounced differences were observed in CD8+ T cells resulting from a combination of LIV and PD-1 blockade. For C-TILs, the reduction in the proportions of CD8+ T cells between PD-1 blockade and no blockade conditions was not significant. PD-1 blockade alone resulted in significantly lower proportions of CD8+ T cells compared to no PD-1 blockade; however, the combination of LIV and PD-1 blockade led to a significant increase in CD8+ T cell proportions compared to PD-1 blockade alone (Fig. 4F). On the other hand, the proportions of unconventional double negative (DN) and double positive (DP) T cells were generally lower under PD-1 blockade, although the differences did not reach statistical significance (Supplementary Fig. 1). Furthermore, PD-1 blockade did not significantly alter the relative proportions of exhausted $PD\text{-}1^+CD4^+$ T cells, $PD\text{-}1^+CD8^+$ T cells, and, $FOXP3^+CD4^+$ regulatory T cells in expanded TILs (Fig. 4, G to I).

Figure on the next page

Fig. 4 | PD-1 blockade synergizes with LIV to increase TIL yields and the proportion of $CD8^+$ T cells in TIL products. A, **B** Proportions of (**A**) $CD4^+$ and (**B**) $CD8^+$ T cells expressing immune checkpoint blockade molecules PD-1 or CTLA-4 from tumor digests. **C** TIL yields in control (C-TIL) and LIV-treated (L-TIL) cultures, with PD-1 blockade via nivolumab (nivo) supplementation or without PD-1 blockade (no nivo). **D** Contour plots of a representative sample showing the proportions of $CD4^+$, $CD8^+$, double-negative (DN), and double-positive (DP) T cells, under the same conditions. **E** Relative proportions of $CD4^+$ T cells in C-TILs and L-TILs, with or without PD-1 blockade. **F** Relative proportions of $CD8^+$ T cells in C-TILs and L-TILs, with or without PD-1 blockade. **G**, **H** Relative proportions of (**G**) $PD\text{-}1^+CD4^+$ T cells and (**H**) $PD\text{-}1^+CD8^+$ T cells in C-TILs and L-TILs, with or without PD-1 blockade. **I** Relative proportions of regulatory $FOXP3^+CD4^+$ T cells in the absence or presence of PD-1 blockade. For all three cases (**G**, **H**, **I**) the differences were insignificant. Bars and error bars represent the Mean ± SD of tumor specimens from three different patients. $*p < 0.05$, $**\ p < 0.01$.


A
CD4+ T Cells
% of CD3+CD4+ Cells
PD-1+ CTLA-4+
B
CD8+ T Cells
% of CD3+CD8+ Cells
PD-1+ CTLA-4+
C
TIL Count
LIV
Nivo
D
Control
LIV
Control + Nivo
LIV + Nivo
CD4+ T Cells
DP T Cells
DN T Cells
CD8+ T Cells
24.5%
0.60%
32.5%
42.4%
28.6%
1.03%
14.5%
55.8%
88.5%
0.16%
1.96%
9.35%
72.6%
0.51%
5.15%
21.7%
CD4-APC-A700
CD8-APC-A750
E
CD4+ TILs
% of CD3+ Cells
F
CD8+ TILs
% of CD3+ Cells
G
PD-1+CD4+ TILs
% of CD3+CD4+ Cells
H
PD-1+CD8+ TILs
% of CD3+CD8+ Cells
I
FOXP3+CD4+ TILs
% of CD3+CD4+ Cells

LIV potentiates functional activity of expanded TILs in autologous tumor organoids

To assess whether LIV-induced phenotypic changes are translated into enhanced functional potency, we co-cultured expanded TILs with autologous patient-derived tumor organoids (PDTOs) (Fig. 5A). TIL reactivity was measured by induction of tumor cell apoptosis through caspase-3/7 activation as previously described[29] and by the secretion of IFN-γ, IL-2, and TNF-α. LIV significantly enhanced TIL cytotoxicity: normalized caspase-3/7 fluorescence was significantly higher in L-TIL + PDTO co-cultures relative to C-TIL + PDTO controls (Fig. 5, B and C), indicating that LIV exposure markedly improved the cytotoxic activity of expanded TILs against autologous tumor cells.

LIV also boosted the ability of TILs to secrete effector cytokines. IL-2 was significantly elevated in L-TIL + PDTO co-cultures compared with L-TIL-only cultures from 75% of tumor specimens. In contrast, no such differences were observed between C-TIL + PDTO and C-TIL-only cultures from all 4 tested tumor specimens (Fig. 5D). Similarly, IFN-γ levels were significantly higher in L-TIL + PDTO co-cultures in 50% of tumor specimens (Fig. 5E) compared to 25% of C-TIL + PDTO co-cultures. Moreover, TNF-α levels were elevated in L-TIL+PDTO co-cultures in 75% of tumor specimens (Fig. 5F) compared to 50% of the corresponding C-TIL + PDTO co-cultures.

Taken together, our results show that LIV enhances both the cytotoxic and pro-inflammatory functions of expanded TILs, improving TIL product quality during biomanufacturing for adoptive cell therapy.

LIV modulates the cytokine milieu to support $CD8^+$ T cell expansion and survival

We hypothesized that the beneficial effects of LIV on TIL expansion and phenotype are mediated by changes in the cytokine milieu. To test this, we compared cytokine concentrations in conditioned media from C-TILs and L-TILs using a Luminex multiplex immunoassay with a 27- analyte kit. LIV exposure induced a broad upregulation of cytokine secretion during TIL expansion (Fig. 6A). Specifically, 8 of the 27 measured analytes were significantly elevated in L-TIL conditioned media compared to C-TIL controls: IL-4, IL-5, IL-7, IL-15, IL-17, MIP-1α, MIP-1β, and FGF (Fig. 6, B to I). Notably, the majority of the upregulated cytokines are pro-inflammatory, consistent with an activated T cell phenotype. Of particular relevance, the γc cytokines IL-7 and IL-15 are both significantly increased by LIV ($p<0.05$) and are central to $CD8^+$ T cell biology. IL-7 is critical for T cell survival and homeostatic proliferation, while IL-15 drives the expansion, maintenance, and cytotoxic function of memory $CD8^+$ T cells.

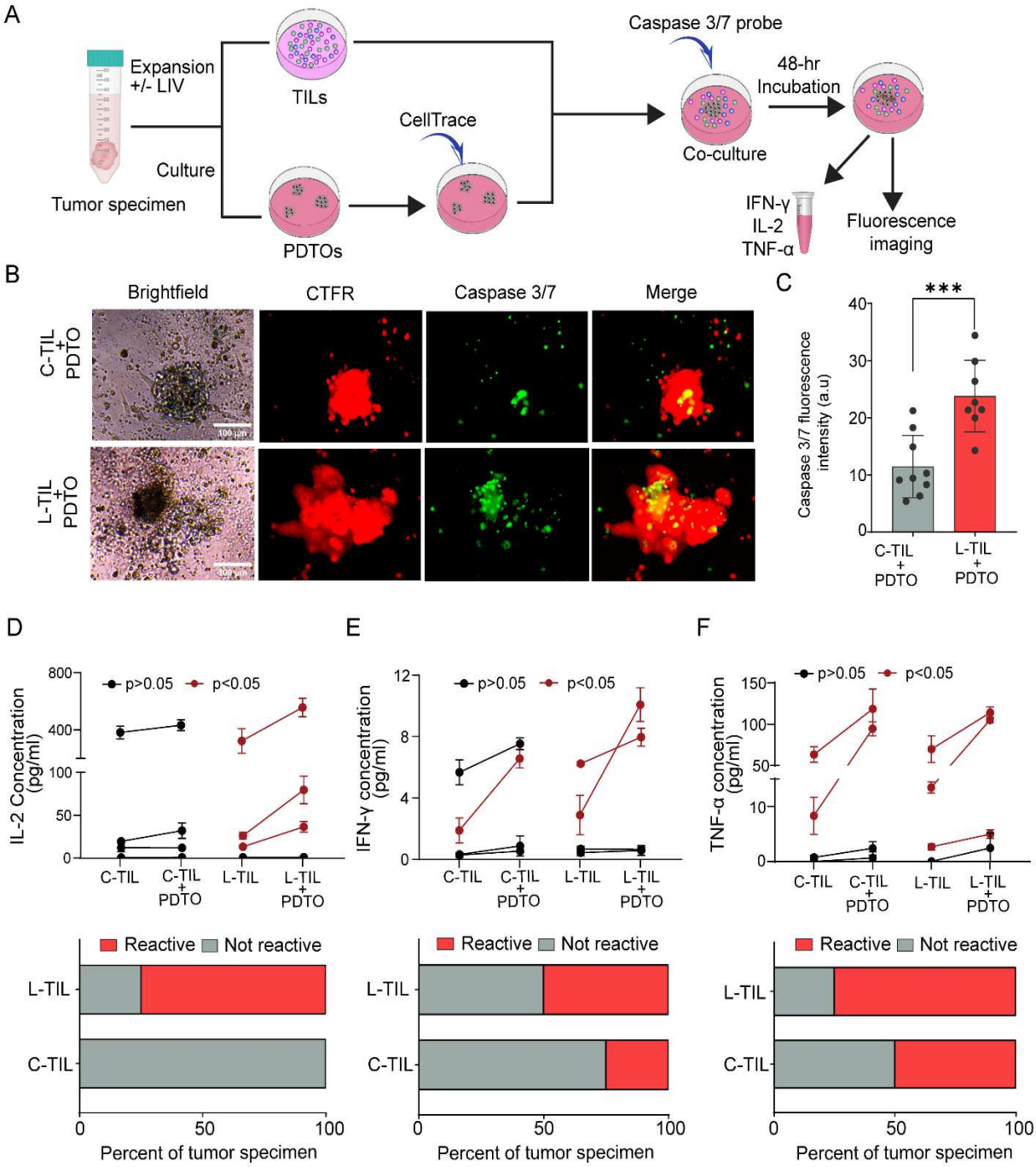


Fig. 5 | Reactivity of expanded TILs in autologous PDTOs. A Experimental schematic. TILs expanded from tumor specimens were co-cultured with autologous CellTrace Far Red-labelled PDTOs at a 10:1 effector-to-target ratio. A caspase 3/7 probe was added at the start of co-culture to visualize tumor cell apoptosis. After 48 hours, fluorescence images were taken and conditioned media were harvested for IL-2, IFN-γ, and TNF-α immunoassays**. B** Representative fluorescence images showing caspase 3/7 activation (apoptosis) in PDTOs after a 48-hour co-culture with autologous TILs. **C** Comparison of caspase 3/7 green dye mean fluorescence intensities (MFI) between C-TIL + PDTO and L-TIL + PDTO co-cultures. Organoids were delineated on brightfield images, and fluorescence intensities (of caspase 3/7 green dye) were quantified using ImageJ. Data points represent area-normalized MFI per single field of view (FOV). Mean ± SD shown, ***$p < 0.001$. **D-F** Comparison of (**D**) IL-2, (**E**) IFN-γ, and (**F**) TNF-α concentrations between conditioned media of C-TIL + PDTO and L-TIL + PDTO co-cultures. Error bars represent Mean ± SD of three replicate experiments per tumor specimen. *$p < 0.01$, **$p < 0.01$, ***$p < 0.001$, ns = not statistically significant.

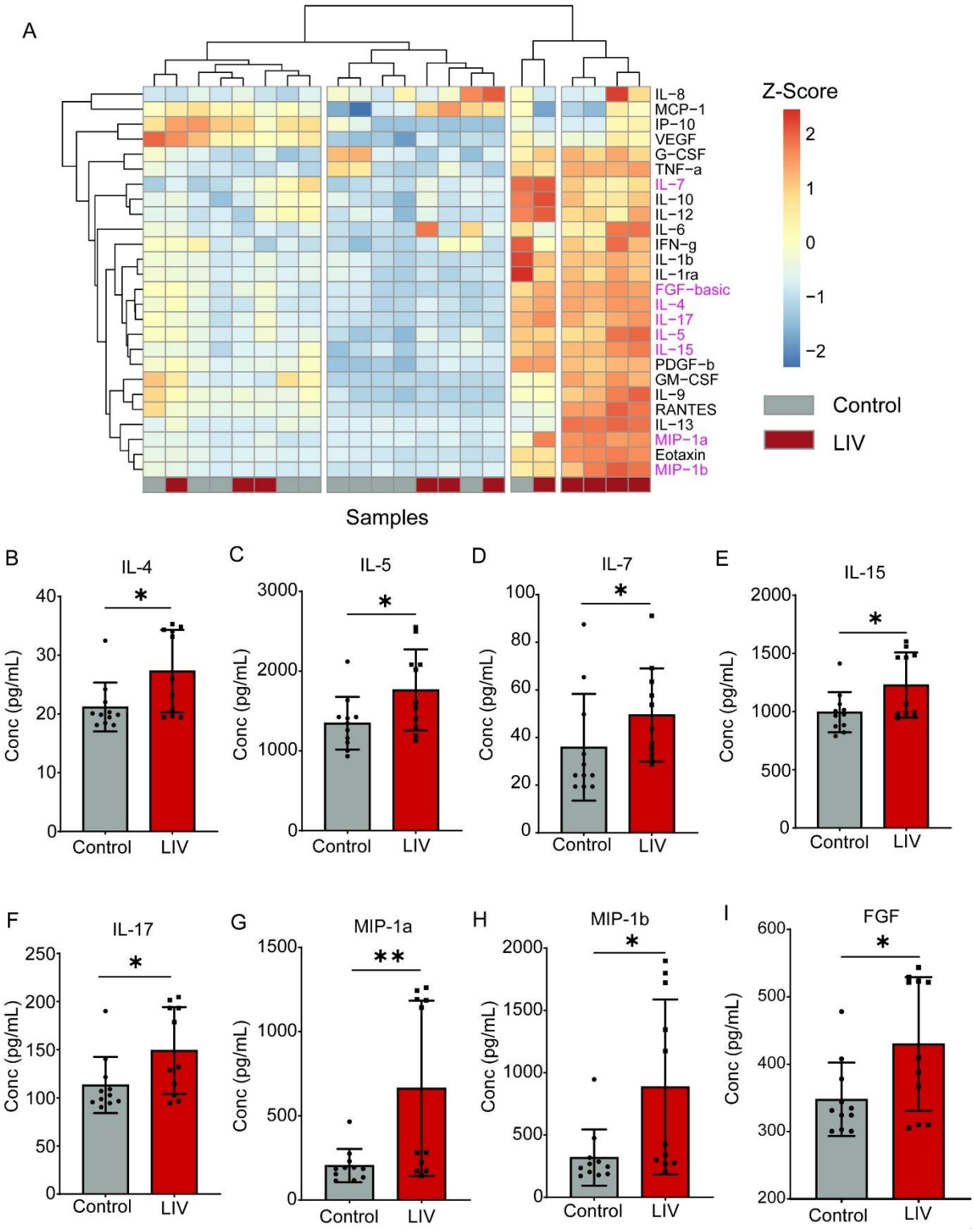


Fig. 6 | LIV alters the cytokine landscape of TIL-conditioned media to support CD8⁺ T cell expansion. Experimental approach: Conditioned media from C-TIL and L-TIL cultures were analyzed using a Luminex multiplex immunoassay panel of 27 analytes. **A** Global cytokine profile: Unsupervised hierarchical clustering heatmap of normalized cytokine concentrations from C-TIL and L-TIL samples. Each column represents an individual sample; each row represents a distinct analyte. Color scale indicates relative cytokine concentration (red = high, blue = low). **B-I** Elevated analytes: Eight analytes were significantly elevated in L-TIL compared to C-TIL conditioned media: (**B**) IL-4, (**C**) IL-5, (**D**) IL-7, (**E**) IL-15, (**F**) IL-17, (**G**) MIP-1α, (**H**) MIP-1β, and (**I**) FGF. Statistics: Data are presented as Mean ± SD of three independent biological replicates. *$p < 0.05$, **$p < 0.01$.

Our data support a model in which LIV enhances the TIL expansion microenvironment through an upregulation of pro-inflammatory cytokines, particularly IL-7 and IL-15. This, in turn, creates a niche that selectively promotes $CD8^+$ T cell expansion and functional maturation.

Discussion

Extending TIL therapy beyond melanoma requires overcoming biomanufacturing bottlenecks caused by tumor immune heterogeneity and unpredictable biochemical strategies. Here, we show that LIV, a biomechanical signal, enhances TIL expansion and functional quality in soft tissue sarcoma. LIV increases TIL yields while preserving cell viability and integrity. Moreover, LIV enriches $CD8^+$ cytotoxic subsets, mitigates PD-1-driven exhaustion, synergizes with PD-1 blockade, and boosts tumor-killing capacity in patient-derived tumor organoids. These results underscore the translational potential of LIV to overcome the challenges of TIL manufacturing from solid tumor specimens.

The mechanisms by which LIV enhances TIL yield and function deserve further discussion. Unlike biochemical approaches that directly modulate receptor signaling or metabolic pathways, LIV acts through mechanotransduction, converting external physical stimuli into intracellular signals that influence gene expression, proliferation, and differentiation[30]. Mechanical properties of the environment exert a strong influence on the behavior of T cells through mechanotransduction of forces via the T cell receptor (TCR), coreceptors, mechano-sensitive ion channels and the cytoskeleton[31]. In the context of TIL manufacturing, LIV biomechanical priming may mimic aspects of the physiological mechanical environment encountered by T cells during migration through tissues or interaction with the tumor stroma. Our observation that LIV enriches $CD8^+$ cytotoxic subsets while mitigating PD-1-driven exhaustion suggests that mechanical signals may preferentially support less-differentiated, more functional T cell states. This is consistent with emerging evidence that LIV can shape lymphocyte fate decisions to mitigate acquired dysfunction such as age-related decline in T cell proliferation, activation, and function[32]. Future studies should investigate the mechanotransductive pathways involved, such as Piezo1 ion channels, YAP/TAZ signaling, or cytoskeletal reorganization, to identify molecular targets that could be pharmacologically enhanced to further improve LIV efficacy.

Mechanical stimulation offers a distinct advantage over biochemical stimulation: the ability to finely tune signal strength to elicit precise cellular responses. LIV is a minimally invasive mechanical stimulation technique for modulating cellular phenotypes both in vitro and in vivo[18]. Cellular responses to LIV are governed by two variable factors: (1) stimulus parameters:

frequency, acceleration, and amplitude[33]; and (2) cell-intrinsic properties: size, shape, and elastic modulus[34]. Together, these factors determine the natural frequency of a cell, which is the frequency at which maximum mechanical force is transmitted to the cell[35]. Finite element modeling estimated the natural frequency of T cells to lie between 10 and 100 Hz[35,36]. Supporting this range, prior work reported a 20.3% increase in Jurkat cell proliferation using 30 Hz, 0.7g LIV signals[37].

In this study, we explored vibration frequencies at the lower end of this range to identify optimal LIV parameters for TIL expansion. We observed a steady improvement in TIL proliferation from 20 to 40 Hz, beyond which the benefits declined, revealing a defined mechanobiological *sweetspot*. Importantly, LIV did not affect cell viability or size, indicating that cells were not subjected to undue stress that could compromise functionality. The observed proliferative improvements can be explained by mechanotransduced forces enhancing T cell activation and proliferation[37]. Based on these findings, we identify 40 Hz as the optimal LIV frequency, providing a reproducible parameter suitable for clinical-grade TIL manufacturing.

The proportion of $CD8^+$ T cells in the final TIL product is a key determinant of therapeutic efficacy, as these cells serve as the primary effectors of tumor clearance[4,38,39]. However, standard TIL expansion protocols under conventional high-dose IL-2 supplementation often enrich $CD4^+$ T cells rather than $CD8^+$ cytotoxic subsets[40]. Several biochemical strategies, including CTLA-4 blockade[16], TGF-β1 supplementation[41], and 4-1BB co-stimulation[42], have been reported to increase the $CD8^+$ T cell proportions during TIL expansion. However, these approaches face translational hurdles related to scaling-up and prohibitive costs. In this study, we investigated whether LIV could positively modulate $CD8^+$ T cell proportions in expanded TILs. Our results support the hypothesis that LIV significantly increased $CD8^+$ T cell proportions in expanded TILs without amplifying Tregs. This selective skewing toward cytotoxic effectors while restraining Treg expansion aligns with the established role of Piezo1-mediated mechanotransduction in enhancing cytotoxic T cell activation and limiting Treg proliferation [27]. Collectively, these findings suggest that LIV offers a scalable, cost-effective, and chemically agnostic alternative to existing biochemical strategies for optimizing TIL product composition.

T cell exhaustion remains a fundamental obstacle in adoptive cell therapy. Prolonged in vitro expansion drives T cells toward a dysfunctional state characterized by impaired cytotoxicity, reduced cytokine secretion, and ultimately, diminished therapeutic efficacy[43]. Our data indicate that LIV mitigates this trajectory. Compared to conventional expansion, LIV generated TIL products with significantly lower proportions of both $PD\text{-}1^+CD4^+$ and $PD\text{-}1^+CD8^+$ exhausted subsets. This anti-exhaustion effect aligns with emerging evidence that

mechanically transduced signaling pathways positively influence T cell function – shaping $CD4^+$ secretory profiles and reinforcing $CD8^+$ T cell activation pathways[28]. Crucially, the LIV-mediated reduction in PD-1^+ cells is not merely a compositional change but likely a functional one. Lower PD-1 expression may render TILs less susceptible to tumor-mediated suppression and more responsive to PD-1 checkpoint blockade[43], a synergy we observed in our autologous organoid models. Thus, by addressing exhaustion at the manufacturing stage, LIV offers a strategy to improve TIL quality before infusion, complementing rather than replacing post-infusion checkpoint inhibition.

Given the clinical success of checkpoint inhibitors, we investigated whether LIV could complement PD-1 blockade during TIL expansion. PD-1 blockade alone produced a trade-off: increased yields at the expense of $CD4^+$ skewing. In contrast, the combination of LIV with PD-1 blockade amplified $CD8^+$ T cell proportions while further improving overall yields. Such synergy suggests that LIV establishes a cytokine and metabolic milieu that enables checkpoint blockade to act more effectively, potentially by creating a more permissive environment for $CD8^+$ T cell expansion. These findings carry direct clinical implications, as PD-1 inhibitors are already integrated into standard cancer therapy and could be readily paired with mechanical stimulation during TIL manufacturing protocols without additional regulatory hurdles. Beyond compositional advantages, LIV-expanded TILs showed improved functional capacity. They induced superior tumor cell apoptosis and secreted higher levels of effector cytokines, including IFN-γ, IL-2, and TNF-α, which are hallmarks of robust antitumor activity. Notably, these functional improvements aligned closely with the observed phenotypic changes: $CD8^+$ T cell enrichment and reduced PD-1^+ exhaustion. The use of PDTOs provides compelling translational validation for these findings, as these models preserve the architectural and cellular heterogeneity of autologous tumors[44], providing a clinically relevant platform for assessing TIL potency.

The biology of T cells, including their activation, proliferation, survival, and effector functions, is profoundly shaped by the cytokine milieu. Among the most critical regulators are the common γ_c cytokines: IL-2, IL-4, IL-7, IL-9, IL-15, and IL-21, which differentially regulate the fate and function of T cell subsets[45,46]. Our cytokine profiling revealed enrichment of pro-inflammatory cytokines in the conditioned media of LIV-treated TILs. Notably, among the upregulated factors were the γ_c cytokines IL-4, IL-7, and IL-15, which exert a strong influence on $CD8^+$ T cell activation, proliferation, survival, and effector functions[46]. The significant LIV-mediated elevation of these γ_c cytokines offers a plausible mechanistic explanation for our key observations. Enhanced IL-7 and IL-15 signaling promotes $CD8^+$ over $CD4^+$ T cell expansion

and functional fitness. This model positions LIV as an upstream biomechanical regulator of the cytokine network; distinct from, and potentially complementary to, direct cytokine supplementation strategies.

The current study has several limitations worth acknowledging. First, our investigation focused primarily on sarcoma-derived TILs; therefore, testing across additional tumor types, including carcinomas of the lung, breast, and gastrointestinal tract, will be needed to establish if our findings generalize to other tumor types. Second, while our cytokine profiling provides valuable mechanistic clues, the definitive molecular pathways underlying LIV-mediated T cell reprogramming remain to be fully delineated. Future studies should systematically dissect the roles of YAP/TAZ transcriptional regulators, mechanosensitive ion channels such as Piezo1, and cytoskeletal dynamics in mediating the effects of LIV on T cell phenotype and function. Third, while our patient-derived organoid models offer robust translational validation ex vivo, in vivo evaluation of TIL persistence, tumor trafficking, and therapeutic efficacy in preclinical animal models will be essential prior to clinical translation. Addressing these limitations will be an important next step toward establishing LIV as a viable component of clinical-grade TIL manufacturing.

Methods

Biological samples and ethics approval

Soft tissue sarcoma (STS) specimens were obtained from the Affiliated Hospital of Jiangxi University of Chinese Medicine. Tissue collection was performed in compliance with all applicable laws and regulations. Written informed consent was obtained from all patients before surgery. The study protocol was approved by the Institutional Review Board of the Affiliated Hospital of Jiangxi University of Chinese Medicine (approval number: JZFYLL20250103001).

A total of 10 tumor specimens, all histologically confirmed STS were obtained and used in all experiments done in this study (Table 1). A combination of lineage differentiation markers including markers of epithelial (PCK and EMA), fibrohistiocytic (Vimentin and CD68), endothelial (ERG and CD34) nerve sheath (S-100 and SOX10), and muscular (SMA, Desmin, and Myf4) were evaluated by immunohistochemistry and utilized to define the sarcoma subtypes.

Media and solution formulation

Tumor tissue collection medium (TTCM) was prepared by supplementing RPMI 1640 (Hyclone)

Table 1 | Patient demographics and immunohistochemical markers of cell lineage in soft-tissue sarcomas

Specimen ID	Age	Sex	Histological Sub-type	Anatomical site	Lineage Differentiation Markers										
					PCK	EMA	Vim	CD68	ERG	CD34	S-100	SOX10	SMA	Des	Myf4
SARC_01	72	F	Pleomorphic dermal sarcoma	Dorsum of the right foot	–	–	+	+		+	–	–	+	+	
SARC_02	79	F	Well-differentiated liposarcoma	Right thigh			+				+				
SARC_03	78	M	High-grade myxofibrosarcoma	Right shank	+	+	+	–	–	+	–		–	+	–
SARC_04	50	M	Leiomyosarcoma	Lower left femur	–	–	+			–	–		+	+	
SARC_05	53	M	Myxoid liposarcoma	Right shank	–		+			+	+				
SARC_06	48	F	Undifferentiated pleomorphic sarcoma	Left thigh	–		+	+	–	–	–	–	+	–	–
SARC_07	48	M	Undifferentiated pleomorphic sarcoma	Right shoulder	–		+	+	–	–	–		+	+	
SARC_08	57	F	Myxoid liposarcoma	Pelvic floor						+	+				
SARC_09	66	M	Myxoid liposarcoma	Popliteal fossa	–		+			+	+				
SARC_10	69	F	Well-differentiated liposarcoma	Right leg	–		+			+	+		–	–	

+ Positive, – Negative

with 10% fetal bovine serum (Invitrogen) and 1% penicillin–streptomycin (Gibco). Tumor tissue digestion reagent (TTDR) consisted of a cocktail of 0.6 mg/mL Dispase (Sigma), 0.6 mg/mL type IV collagenase (Sigma), and 0.01 mg/mL DNase I (Sigma) in RPMI 1640 medium (Hyclone) supplemented with 10% fetal bovine serum (Invitrogen). TIL isolation medium was prepared by supplementing RPMI 1640 medium (Hyclone) with 7.5% human serum AB (Gemini), 1% penicillin–streptomycin (Gibco), 2 mM L-glutamine (Sigma), 6000 IU/mL recombinant human IL-2 (PeproTech), and 1 μg/mL Normocin (Invivogen). Patient-derived tumor organoid culture medium consisted of complete MammoCult medium (StemCell) supplemented with 1% penicillin–streptomycin (Gibco) and 1 μg/mL Normocin (Invivogen).

Expansion of TILs from tumor specimens

Tumor fragments were washed five times with DPBS supplemented with 2% FBS and 1% penicillin–streptomycin. After the final wash, tumor fragments were transferred to a 100 × 20 mm cell culture dish, and the fat and connective tissues were removed using sterile scalpels and forceps. The tumor fragments were then minced into small pieces of approximately 1–2

mm^3. Two milliliters of pre-warmed TIL isolation medium were added to each well of a 24-well cell culture plate, and one tumor piece was transferred to each well using sterile forceps. This was followed by the addition of 6000 IU/mL recombinant human IL-2 to each well and mixing by pipetting (two times). The plate was then incubated at 37°C with 5% CO_2.

Half of the culture medium was replaced every three days. This was achieved by tilting the plate and carefully aspirating 1 mL of medium without disturbing the bottom of the well. Freshly prepared, pre-warmed TIL isolation medium (1 mL) supplemented with 6000 IU/mL IL-2 was then added. TILs were monitored for growth and contamination by inverted microscopy. Wells were split upon reaching approximately 80% confluence by removing the tumor fragment, resuspending TILs by pipetting, and transferring 0.5 mL of the TIL suspension to new wells. Tumor fragments were maintained in culture for a maximum of 14 days. Mycoplasma contamination was assessed using the Mycostrip mycoplasma detection kit (Invivogen), in accordance with the manufacturer's protocol.

Experimental set-up for delivery of LIV

LIV was delivered using a loudspeaker-based vibration device driven by a function generator (3B Scientific, Germany) (Supplementary Fig. 2A). Cell culture plates were secured onto the vibrating platform using clothespins (Supplementary Fig. 2B). The device was calibrated with a vibrometer to confirm that the vibration intensity remained within the expected range (Supplementary Fig. 2C). Two 24-well plates of TIL cultures were prepared. One plate, designated as the treatment group, received LIV for seven consecutive days beginning on day 1 of TIL expansion. The second plate served as a control and was handled identically but without LIV exposure. Both plates were placed in a biosafety cabinet during LIV delivery, with the control plate remaining in the cabinet for the same duration as the treatment plate.

Optimization of LIV parameters

To determine the optimal LIV parameters, 24 tumor fragments were cultured for two days in TIL isolation medium to allow TIL extravasation. On day two, extravasated TILs were pooled, counted, and assessed for viability using a trypan blue exclusion assay. TILs were then seeded at 100,000 viable cells per 30 mm dish in 2 mL of fresh TIL isolation medium (RPMI 1640 supplemented with 7.5% human AB serum, 1% penicillin–streptomycin, 2 mM L-glutamine, and 6000 IU/mL recombinant human IL-2). Fifteen dishes were divided into five groups ($n = 3$ per group), each subjected to LIV treatment at frequencies of 0 Hz (control), 20 Hz, 30 Hz, 40 Hz, and 50 Hz, with acceleration fixed at 0.7g. LIV was delivered in two 20-m bouts per day,

separated by a 2- h interval. After five days of treatment, cells were harvested and counted using an iCytal automatic cell counter (Ultrassay Biotech) to determine cell number, viability, and cell size.

Flow cytometry

Single-cell suspensions of tumor digests and expanded TILs were analyzed by flow cytometry to characterize T cell populations. Cells were stained with antibodies against CD3-FITC (OKT3), CD4-APC (OKT4), CD8-APC-eFluor 780 (RPA-T8), CD152-PE (14D3), CD279-PerCP-eFluor 710 (MIH4), and FOXP3-PE-Cyanine7 (PCH101) (all eBioscience, dilutions 1:20 except CD4 at 1:100). Cell viability was assessed using fixable viability dye eFluor 450 (Invitrogen, cat. 65-0863-14). Intracellular staining was performed after fixation and permeabilization with the Foxp3/Transcription Factor Staining Buffer Set (eBioscience, cat. 00-5523-00) for 30 m at room temperature. Fluorescence Minus One (FMO) controls were used for CD152, CD279, and FOXP3 to guide gating. To compensate for fluorescence spillover, antibody capture beads (Invitrogen cat. 01-2222-42) were used for all fluorophore-conjugated antibodies, and an aliquot of cells was used to compensate for the fixable viability dye. Data were acquired on a CytoFLEX flow cytometer (Beckman Coulter, Indianapolis, IN) and analyzed using FlowJo 10.1 software (Waters Biosciences). The gating strategy (Supplementary Fig. 3) was used to define distinct T cell populations.

Generation of patient-derived tumor organoids (PDTOs)

Tumor specimens were enzymatically digested with type I collagenase (0.6 mg/mL), Dispase (0.6 mg/mL), and DNase I (0.01 mg/mL) to obtain single-cell suspensions. An aliquot of single-cell suspension containing 1×10^6 cells was used for PDTO generation. Cells were centrifuged at 600g for 5 m, the supernatant was carefully aspirated, and the cell pellet was resuspended in 300 µL of cold MammoCult medium on ice in a pre-chilled 1.5 mL Eppendorf tube. Subsequently, 400 µL of Matrigel was added to the cell suspension to achieve a total volume of 700 µL, and the mixture was pipetted multiple times to ensure homogeneous mixing. The mixture was kept on ice, and Matrigel domes were plated immediately. Using a P20 pipette fitted with a low-attachment 300 µL tip, 15 µL of the cell suspension was aspirated and gently plated as domes in a pre-warmed 12-well plate (3–4 domes per well). The culture plate was immediately transferred to a humidified 37 °C incubator with 5% CO_2 and incubated for 30 m to allow dome solidification. After the domes were visibly solidified, 1 mL of pre-warmed MammoCult medium was added dropwise along the sides of each well using a P1000 pipette.

The plate was then returned to the humidified 37 °C incubator with 5% CO_2, and organoid growth was monitored daily by inverted microscopy. Organoids were passaged weekly by mechanical dissociation. During passaging, Matrigel domes were disrupted by flushing with ice-cold DMEM+++ (DMEM supplemented with GlutaMAX, HEPES, and penicillin–streptomycin) to recover the organoids. Organoids were mechanically split by passing them 5–10 times through a sterile 10 µL pipette tip attached to a 5 mL glass Pasteur pipette. After 3–4 passages, organoids were cryopreserved in liquid nitrogen for future use.

Co-culture of TILs and PDTOs

Organoids were harvested following the passaging procedure described above. An aliquot of the organoid suspension was dissociated into single cells and counted to determine the number of tumor cells, enabling calculation of an effector-to-target (E:T) ratio of 10:1. Tumor organoids were then resuspended in organoid culture medium and seeded in a flat-bottom 96-well plate. After three days, autologous TILs were added to initiate organoid co-culture. TIL-only wells served as controls for cytokine secretion. Prior to co-culture, organoids were pre-stained with 1 µM CellTrace Far Red (Invitrogen) to facilitate visualization. At the start of co-culture, a caspase-3/7 probe was added at a 1:2000 dilution to monitor cell apoptosis. After 48 h, fluorescence images were acquired to assess apoptosis. Conditioned media were harvested for multiplex immunoassays of IFN-γ, TNF-α, and IL-2.

Quantification of caspase 3/7 fluorescence of single organoids in fluorescence microscopy

Apoptosis induction in PDTOs was quantified from fluorescence images using ImageJ software, following a previously reported workflow[47]. Using the freehand selection tool in ImageJ, individual organoids were manually delineated on brightfield images to generate regions of interest (ROIs). These ROIs were then mapped onto the corresponding caspase-3/7 green fluorescence channel. For each ROI, the mean gray value and area were measured to compute the area-normalized fluorescence intensity. Background correction was performed by subtracting the mean gray value measured from representative background areas.

Luminex immunoassays of cytokines and chemokines

Cytokine and chemokine concentrations in conditioned culture media were measured using the Bio-Plex Pro Human Cytokine 27-plex Assay Kit (Bio-Rad, Carlsbad, CA, USA) in accordance with the manufacturer's protocol. Briefly, conditioned media were prepared by centrifugation at 1000 g for 15 m at 4 °C. Samples were then diluted two-fold by adding an equal volume of

sample diluent. An 8-point, four-fold serial dilution series of the standard was prepared. In the first tube, 50 µL of standard was added to 150 µL of standard diluent, yielding a total volume of 200 µL and a four-fold dilution factor. Subsequently, 50 µL from the first tube was transferred to the second tube containing 150 µL of diluent, and this process was repeated sequentially through the eighth tube. Magnetic beads coupled with capture antibodies were washed and incubated with samples or standards to allow capture of analytes. After washing the assay plate, detection antibodies were added, followed by additional wash steps and the addition of streptavidin-phycoerythrin (SA-PE). Fluorescence intensities (FI) of detecting antibodies and SA-PE were acquired on a LUMINEX 200 analyzer (Bio-Rad, Carlsbad, CA, USA). Cytokine and chemokine concentrations in samples were calculated by the acquisition software and exported for further analysis.

Statistical analysis

All statistical analyses were performed using GraphPad Prism 8.0 software. Data are presented as means and standard deviations (SD) or means and standard errors of the mean (SEM) from at least three independent experiments. Normality of data distribution was assessed using the Shapiro–Wilk test. Statistical significance was determined using the paired t-test, Wilcoxon matched-pairs signed-rank test, one-way analysis of variance (ANOVA), or two-way ANOVA, as appropriate. Significance was defined as $p < 0.05$, with asterisks denoting p-values: ns (not significant), *$p < 0.05$, **$p < 0.01$, ***$p < 0.001$, and ****$p < 0.0001$.

Data availability

All data in our study are available upon request.

References

1. Zhang, P., Zhang, G. & Wan, X. Challenges and new technologies in adoptive cell therapy. *J Hematol Oncol* **16**, 97 (2023). https://doi.org:10.1186/s13045-023-01492-8
2. Medina, T. *et al.* Long-Term Efficacy and Safety of Lifileucel Tumor-Infiltrating Lymphocyte Cell Therapy in Patients With Advanced Melanoma: A 5-Year Analysis of the C-144-01 Study. *J Clin Oncol* **43**, 3565-3572 (2025). https://doi.org:10.1200/jco-25-00765
3. Wang, S. *et al.* Perspectives of tumor-infiltrating lymphocyte treatment in solid tumors. *BMC Med* **19**, 140 (2021). https://doi.org:10.1186/s12916-021-02006-4
4. Radvanyi, L. G. *et al.* Specific lymphocyte subsets predict response to adoptive cell therapy using expanded autologous tumor-infiltrating lymphocytes in metastatic melanoma patients. *Clin Cancer Res* **18**, 6758-6770 (2012). https://doi.org:10.1158/1078-0432.Ccr-12-1177
5. Hu, W., Bian, Y. & Ji, H. TIL Therapy in Lung Cancer: Current Progress and Perspectives. *Adv Sci (Weinh)* **11**, e2409356 (2024). https://doi.org:10.1002/advs.202409356
6. Chen, R., Johnson, J., Rezazadeh, A. & Dudek, A. Z. Tumour-infiltrating lymphocyte therapy landscape: prospects and challenges. *BMJ Oncol* **4**, e000566 (2025). https://doi.org:10.1136/bmjonc-2024-000566

7. Wiertsema, P., Tan, Y. H., Haanen, J., Seijkens, T. T. P. & Jedema, I. Advances in TIL therapy: Expanding the horizons beyond melanoma. *Med* **6**, 100702 (2025). https://doi.org:10.1016/j.medj.2025.100702
8. Singh, K. *et al.* IL-7-mediated expansion of autologous lymphocytes increases CD8+ VLA-4 expression and accumulation in glioblastoma models. *J Clin Invest* **135** (2025). https://doi.org:10.1172/jci181471
9. Arruda, L. C. *et al.* Multiple infusions of TILs expanded with IL-2/IL-15/IL-21 lead to an improved PK/PD profile and long-term clinical responses in patients with cold tumors. *Cytotherapy* **27**, S165 (2025). https://doi.org:https://doi.org/10.1016/j.jcyt.2025.03.331
10. Aehnlich, P., Carnaz Simões, A. M., Skadborg, S. K., Holmen Olofsson, G. & Thor Straten, P. Expansion With IL-15 Increases Cytotoxicity of Vγ9Vδ2 T Cells and Is Associated With Higher Levels of Cytotoxic Molecules and T-bet. *Front Immunol* **11**, 1868 (2020). https://doi.org:10.3389/fimmu.2020.01868
11. Kalaitsidou, M. *et al.* Signaling via a CD28/CD40 chimeric costimulatory antigen receptor (CoStAR™), targeting folate receptor alpha, enhances T cell activity and augments tumor reactivity of tumor infiltrating lymphocytes. *Front Immunol* **14**, 1256491 (2023). https://doi.org:10.3389/fimmu.2023.1256491
12. Shah, P. *et al.* Combined IL-2, agonistic CD3 and 4-1BB stimulation preserve clonotype hierarchy in propagated non-small cell lung cancer tumor-infiltrating lymphocytes. *J Immunother Cancer* **10** (2022). https://doi.org:10.1136/jitc-2021-003082
13. Campos Carrascosa, L. *et al.* FcγRIIB engagement drives agonistic activity of Fc-engineered αOX40 antibody to stimulate human tumor-infiltrating T cells. *J Immunother Cancer* **8** (2020). https://doi.org:10.1136/jitc-2020-000816
14. Scheffel, M. J. *et al.* N-acetyl cysteine protects anti-melanoma cytotoxic T cells from exhaustion induced by rapid expansion via the downmodulation of Foxo1 in an Akt-dependent manner. *Cancer Immunol Immunother* **67**, 691-702 (2018). https://doi.org:10.1007/s00262-018-2120-5
15. Scheffel, M. J. *et al.* Efficacy of Adoptive T-cell Therapy Is Improved by Treatment with the Antioxidant N-Acetyl Cysteine, Which Limits Activation-Induced T-cell Death. *Cancer Res* **76**, 6006-6016 (2016). https://doi.org:10.1158/0008-5472.Can-16-0587
16. Friese, C. *et al.* CTLA-4 blockade boosts the expansion of tumor-reactive CD8(+) tumor-infiltrating lymphocytes in ovarian cancer. *Sci Rep* **10**, 3914 (2020). https://doi.org:10.1038/s41598-020-60738-4
17. Lak, S. *et al.* Combined PD-L1 and TIM3 blockade improves expansion of fit human CD8(+) antigen-specific T cells for adoptive immunotherapy. *Mol Ther Methods Clin Dev* **27**, 230-245 (2022). https://doi.org:10.1016/j.omtm.2022.09.016
18. Johnson-Love, O., Salmeron-Sanchez, M., Reid, S., Childs, P. G. & Dalby, M. J. Vibration-based cell engineering. *Nature Reviews Bioengineering* **3**, 408-429 (2025). https://doi.org:10.1038/s44222-025-00273-x
19. Jeffreys, N., Brockman, J. M., Zhai, Y., Ingber, D. E. & Mooney, D. J. Mechanical forces amplify TCR mechanotransduction in T cell activation and function. *Appl Phys Rev* **11**, 011304 (2024). https://doi.org:10.1063/5.0166848
20. Basu, R. *et al.* Cytotoxic T Cells Use Mechanical Force to Potentiate Target Cell Killing. *Cell* **165**, 100-110 (2016). https://doi.org:10.1016/j.cell.2016.01.021
21. Hu, K. H. & Butte, M. J. T cell activation requires force generation. *J Cell Biol* **213**, 535-542 (2016). https://doi.org:10.1083/jcb.201511053
22. Wu, X. & Ye, Z. Mechanoimmunology of T-Cell Activation. *Scand J Immunol* **101**, e70009 (2025). https://doi.org:10.1111/sji.70009
23. Majedi, F. S. *et al.* Augmentation of T-Cell Activation by Oscillatory Forces and Engineered Antigen-Presenting Cells. *Nano Lett* **19**, 6945-6954 (2019). https://doi.org:10.1021/acs.nanolett.9b02252
24. Hope, J. M. *et al.* Fluid shear stress enhances T cell activation through Piezo1. *BMC Biol* **20**, 61 (2022). https://doi.org:10.1186/s12915-022-01266-7
25. Liu, C. S. C. *et al.* Cutting Edge: Piezo1 Mechanosensors Optimize Human T Cell Activation. *The Journal of Immunology* **200**, 1255-1260 (2018). https://doi.org:10.4049/jimmunol.1701118
26. Mikosik, A. *et al.* Roles of calpain-calpastatin system (CCS) in human T cell activation. *Oncotarget* **7**, 76479-76495 (2016). https://doi.org:10.18632/oncotarget.13259
27. Jairaman, A. *et al.* Piezo1 channels restrain regulatory T cells but are dispensable for effector CD4(+) T cell responses. *Sci Adv* **7** (2021). https://doi.org:10.1126/sciadv.abg5859
28. Abiff, M. *et al.* Piezo1 facilitates optimal T cell activation during tumor challenge. *Oncoimmunology* **12**, 2281179 (2023). https://doi.org:10.1080/2162402x.2023.2281179
29. Shim, M. K. *et al.* Caspase-3/-7-Specific Metabolic Precursor for Bioorthogonal Tracking of Tumor Apoptosis. *Sci Rep* **7**, 16635 (2017). https://doi.org:10.1038/s41598-017-16653-2
30. del Rosario-Gilabert, D., Valenzuela-Miralles, A. & Esquiva, G. Advances in mechanotransduction and sonobiology: effects of audible acoustic waves and low-vibration stimulations on mammalian cells.

Biophysical Reviews **16**, 783-812 (2024). https://doi.org:10.1007/s12551-024-01242-1
31. Zubia-Aranburu, J., Zhang, L. & Dong, M. T-cell mechanobiology: How molecular forces shape immune function. *Journal of Cell Biology* **225** (2026). https://doi.org:10.1083/jcb.202601058
32. Ashdown, C. P. *et al.* Low intensity vibration as a novel strategy to normalize age-related deficits in T cell proliferation, activation, and function. *Scientific Reports* **16**, 9428 (2026). https://doi.org:10.1038/s41598-026-40154-w
33. Wang, L., Hsu, H. Y., Li, X. & Xian, C. J. Effects of Frequency and Acceleration Amplitude on Osteoblast Mechanical Vibration Responses: A Finite Element Study. *Biomed Res Int* **2016**, 2735091 (2016). https://doi.org:10.1155/2016/2735091
34. Ku, B. *et al.* Effect of elastic modulus of tumour and non-tumour cells on vibration-induced behaviours. *Sci Rep* **15**, 13199 (2025). https://doi.org:10.1038/s41598-025-97837-z
35. Xiong, X. *et al.* Enhancing anti-tumor potential: low-intensity vibration suppresses osteosarcoma progression and augments MSCs' tumor-suppressive abilities. *Theranostics* **14**, 1430-1449 (2024). https://doi.org:10.7150/thno.90945
36. Xiong, X. *et al.* Therapeutic Insights into Low-intensity Vibration for Generating Induced Tumor-Suppressive Cells and Modulating the Bone Microenvironment. *Engineering* **43**, 210-224 (2024).
37. Chan, M. E. *et al.* Low intensity mechanical signals promote proliferation in a cell-specific manner: Tailoring a non-drug strategy to enhance biomanufacturing yields. *Mechanobiol Med* **2** (2024). https://doi.org:10.1016/j.mbm.2024.100080
38. Chacon, J. A. *et al.* Manipulating the tumor microenvironment ex vivo for enhanced expansion of tumor-infiltrating lymphocytes for adoptive cell therapy. *Clin Cancer Res* **21**, 611-621 (2015). https://doi.org:10.1158/1078-0432.Ccr-14-1934
39. Liu, S. *et al.* TGF-beta1 induces preferential rapid expansion and persistence of tumor antigen-specific CD8+ T cells for adoptive immunotherapy. *J Immunother* **33**, 371-381 (2010). https://doi.org:10.1097/CJI.0b013e3181cd1180
40. Chacon, J. A. *et al.* Co-stimulation through 4-1BB/CD137 improves the expansion and function of CD8(+) melanoma tumor-infiltrating lymphocytes for adoptive T-cell therapy. *PLoS One* **8**, e60031 (2013). https://doi.org:10.1371/journal.pone.0060031
41. Zhou, X., Wu, J., Duan, C. & Liu, Y. Retrospective Analysis of Adoptive TIL Therapy plus Anti-PD1 Therapy in Patients with Chemotherapy-Resistant Metastatic Osteosarcoma. *J Immunol Res* **2020**, 7890985 (2020). https://doi.org:10.1155/2020/7890985
42. Thorel, L. *et al.* Patient-derived tumor organoids: a new avenue for preclinical research and precision medicine in oncology. *Exp Mol Med* **56**, 1531-1551 (2024). https://doi.org:10.1038/s12276-024-01272-5
43. Rochman, Y., Spolski, R. & Leonard, W. J. New insights into the regulation of T cells by gamma(c) family cytokines. *Nat Rev Immunol* **9**, 480-490 (2009). https://doi.org:10.1038/nri2580
44. Leonard, W. J., Lin, J. X. & O'Shea, J. J. The γ(c) Family of Cytokines: Basic Biology to Therapeutic Ramifications. *Immunity* **50**, 832-850 (2019). https://doi.org:10.1016/j.immuni.2019.03.028
45. Lievense, J. J. *et al.* Defining the Quality Attributes for Tumor-Infiltrating Lymphocyte Medicinal Products. *Transplant Cell Ther* **31**, S610-s625 (2025). https://doi.org:10.1016/j.jtct.2024.04.015
46. Raskov, H., Orhan, A., Christensen, J. P. & Gögenur, I. Cytotoxic CD8(+) T cells in cancer and cancer immunotherapy. *Br J Cancer* **124**, 359-367 (2021). https://doi.org:10.1038/s41416-020-01048-4
47. Flood, P. & Nally, K. Quantification of Cytokine-Induced Cell Death in Human Colonic Organoids Using Live Fluorescence Microscopy. *J Vis Exp* (2024). https://doi.org:10.3791/66759

Author contributions

G.F.S.: Conception and design; data acquisition; analysis and interpretation of data; writing, review, and revision of manuscript. B.K.K.: Data acquisition; analysis and interpretation; writing, review and revision of manuscript. S.S.M.: Data analysis and interpretation; writing, review and revision of manuscript. W.Z. & Y.Z.: Sample procurement and data acquisition; analysis and interpretation; lab planning and administrative; writing, graphics, revision of manuscript. X.H.: Data acquisition; analysis; writing, review and revision of manuscript; administrative, technical and material support. Y.J.N.: Data acquisition; lab planning and administrative; review of manuscript. Y.W., Q.C. & L.Y.: Sample procurement and data acquisition; administrative and analysis of data; writing and review of manuscript. L.W. & P.L.: Writing, review, and revision of manuscript; administrative, technical, material, and publication support. R.P.S.H.: Conception and design; analysis and interpretation of data; writing, review, and revision of manuscript; administrative, technical, material support; study supervision.

Competing interests
The authors declare no conflict of interest.

Acknowledgements
This work was funded by the National Natural Science Foundation of China (Grant No. 81570061), the Jiangxi University of Chinese Medicine Innovation Team Funding (Grant No. CXTD22018) and the Startup Funds of Jiangxi University of Chinese Medicine Cancer Research Center (Grant No. 12418008). The funders played no role in study design, data collection, analysis and interpretation of data, or the writing of this manuscript. We thank all staff in the Department of Bone & Soft Tissue Oncology, and the Department of Pathology at The Affiliated Hospital of Jiangxi University of Chinese Medicine for patient samples and logistical support.

AI usage statement
We employed DeepSeek solely for improving English writeup – it was not used to generate scientific data, perform analyses, interpret results, or draw conclusions.

Additional information
Supplementary information The online version contains supplementary material available at xxx.

Correspondence and requests for materials should be addressed to
Geofrey F. Soko or Ray P.S. Han.

Supplementary Files

This is a list of supplementary files associated with this preprint. Click to download.

- LIVTILPaperSupplMaterial.docx